Synthesis and Direct Sintering of Nanosized (MIV,MIII)O2- x Hydrated Oxides as Electrolyte Ceramics

Nicolas Clavier, Yanis Cherkaski, Julien Martinez, Sophie Costis, Théo Cordara, F. Audubert, Laurent Brissonneau, Nicolas Dacheux

Synthesis and direct sintering of nanosized $(M^{IV},M^{III})O_{2-x}$ hydrated oxides as electrolyte ceramics

N. Clavier [1,], Y. Cherkaski [1,2], J. Martinez [1,3], S. Costis [1], T. Cordara [1], F. Audubert [4], L. Brissonneau [2], N. Dacheux [1]*

[1] ICSM, Institut de Chimie Séparative de Marcoule, UMR 5257, CEA, CNRS, ENSCM, Univ. Montpellier, Site de Marcoule – Bât. 426, BP 17171, 30207 Bagnols/Cèze, France

[2] CEA/DEN/DTN/SMTA/LIPC, Site de Cadarache, 13108 St-Paul lez Durance, France

[3] CEA/DEN/DMRC/SECA/LFC, Site de Marcoule – Bât. 399, BP 17171, 30207 Bagnols/Cèze, France

[4] CEA/DEN/DEC/SA3C/LAMIR, Site de Cadarache, 13108 St-Paul lez Durance, France

*** Corresponding author :**

Dr. Nicolas CLAVIER
ICSM – UMR 5257, CEA, CNRS, ENSCM, Univ. Montpellier
Site de Marcoule – Bât 426
BP 17171
30207 Bagnols sur Cèze
France

Phone : + 33 4 66 33 92 08
Fax : + 33 4 66 79 76 11

nicolas.clavier@icsm.fr

Abstract :

Highly reactive and nanosized $Th_{1-x}Y_xO_{2-x/2}$ or $Ce_{0.8}Ln_{0.2}O_{1.9}$ mixed oxides were prepared through the initial precipitation of hydroxide precursors which were further dried under vacuum. Whatever the chemical system investigated, the characterization of the powdered samples evidenced a rapid aging process leading to hydrated oxides. The thermal behavior of these samples was further investigated and first showed a two-step dehydration process, with the successive departure of adsorbed then constitutive water, both yielding a drastic drop of the powders reactivity (i.e. decrease of the specific surface area). Sintering experiments were then undertaken by starting directly from raw powders and revealed very rapid densification kinetics. Highly densified pellets (above 95%TD) with a fine grain microstructure were obtained after only 1 hour of heat treatment at 1600°C. This easy and versatile process of precipitation, that can be followed by direct densification of the powders, then appears as a promising option for the elaboration of homogenous ceramic electrolytes.

Keywords :

Thorium – Cerium – Ceramic electrolyte – Oxide – Sintering

1. Introduction

Due to the rarefaction of natural resources and to the considerable increase of the world global demand, the cost of energy, and particularly that of electricity, is planned to rise during the next decades [1]. The development of innovative production sources then appears as one of the XXIth century top challenges, with the aim to provide massive energy supply and still assuming a sustainable politics for resources, notably through the choice of closed-cycles that integrate the recycling of the fuels and various materials involved. In this framework, France already possesses a long-term experience in two main sectors thought to provide promising answers to the energetic issues of the next decades.

First, the historical knowledge acquired in the domain of electronuclear energy is still pursued through the development of new concepts of reactors, called as Generation IV reactors [2]. The Sodium-cooled Fast Reactor (SFR) concept was more particularly selected [3] to provide a sustainable politics regarding uranium resources, for example through the use of depleted uranium as fuel, with improve safety, reliability and resistance to proliferation. In this context, one of the correlated challenges in the material sciences domain is to assess the peculiar chemistry of liquid sodium. Particularly, the oxygen content, which controls the corrosion rate of the stainless steel claddings [4], must be kept under a specific value (usually few ppm), and then monitored through the use of potentiometric sensors. Such systems generally contain a ceramic electrolyte which must be compatible with sodium at high temperature (≈400°C), mechanically resistant and purely ionic conductor [5]. In this aim, several studies already suggested the use of yttrium-doped thoria (i.e. $Th_{1-x}Y_xO_{2-x/2}$) [6]. Indeed, the incorporation of Y^{3+} in the fluorite-type structure of ThO_2 (space group Fm-3m) produces oxygen vacancies which turns the ceramic into an ionic conductor [7] while doped thoria was generally reported to be much less sensitive to sodium corrosion compared to zirconia [8]. It is thus interesting to study new ways of preparation for these mixed oxides, but also to evaluate their ability to sinter in order to optimize their processing as a ceramic material.

On the other hand, the development of fuel cells constitutes from many years a major research effort. This interest has even grown recently due to the possible application of these technologies in the automotive industry and in portable devices. Among the numerous concepts envisaged, Solid Oxide Fuel Cells (SOFC) offer important potentialities due to their

high electrical efficiency and their fuel flexibility. They also provide high electrical power (up to 2MW) [9] but remained associated to high temperatures of operation that can reach 800-1000°C [10]. To lower this temperature, electrolyte materials, which can be seen as the heart of the SOFC unit, are strongly investigated. One can particularly retain fluorite-type materials such as Bi_2O_3, ZrO_2 or CeO_2 [11], which are usually doped with aliovalent cations in order to create oxygen vacancies : a good example is the substitution of the host Ce^{4+} by acceptor cations such as M^{3+} (M = Ln, Y) [12]. Once again, it then appears essential to develop original ways of synthesis that offer the possibility to prepare homogeneous mixed oxides and then to proceed to their densification with the aim to control their final microstructure.

Strong similarities then arise between the $(M^{IV},M^{III})O_{2-x}$ electrolyte ceramic materials used either in the field of nuclear industry or for SOFC units. An interesting point of comparison lies in the preparation methods reported in the literature for such compounds. Indeed, powder metallurgy processes, which are based on the mechanical mixture of parent oxide compounds and subsequent heat treatment are, so far, the most frequently used [13]. Although, the homogeneity of the cation distribution in the fluorite structure remains an important parameter to consider if one wants to optimize the performances of the materials within their life-cycle. As a matter of example, the presence of Ln^{3+}-enriched phases in doped-ceria electrolytes can induce the formation of complex defects that tend to lower the ionic conductivity [14]. Thus, even if the use of wet chemistry methods could ensure the co-precipitation of the various cations considered in homogenous precursor systems, it remains poorly investigated so far. For actinide-based systems, crystallized precursors precipitated at room temperature or in mild hydrothermal conditions were particularly focused on the use of oxalic acid as a complexing agent [15]. Similarly, attempts to prepare homogenous doped-ceria electrolytes mainly concerned sol-gel methods [16]. The development of new ways of preparation based on the direct preparation of mixed-oxides is thus an open field for investigation.

On this basis, the preparation of $Th_{1-x}Y_xO_{2-x/2}$ ($0.01 \leq x \leq 0.22$) and $Ce_{0.8}Ln_{0.2}O_{1.9}$ solid solutions (with Ln = Nd, Sm, Gd) through an hydroxide wet chemistry route was considered in this work [17]. On the one hand, several compositions of yttrium-doped thoria were explored, both below and above the reference value of x = 0.15 corresponding to the optimal ionic conduction reported in the literature [5, 18]. On the other hand ceria doped with 20 mol% in trivalent lanthanides were considered as this peculiar composition was frequently investigated for electrode materials [19]. The high tendency of tetravalent lanthanides and

actinides towards hydroxylation, which was early reported to result in the formation of colloids in solution, further yielding nanoparticles [10, 11], was used in this work to finally obtain carbon-free and highly reactive oxide solid solutions. After the description of the preparation method, this paper reports the characterization through various physico-chemical techniques of the precursors at room temperature as well as during heat treatment leading to oxides. Finally, the densification of the samples through direct sintering of raw powders was investigated through dilatometry and SEM observations.

2. Experimental section

Synthesis of powdered samples.

All the chemicals used, including $Th(NO_3)_4 \cdot 4\text{-}5H_2O$, $Ln(NO_3)_3 \cdot nH_2O$ and $Y(NO_3)_3 \cdot nH_2O$ were of analytical grade and supplied by Sigma-Aldrich. As the nitrate salts are known to be strongly hygroscopic, each powder was dissolved in acidic media (1M HNO_3 solution prepared from concentrated 69.5% HNO_3, Carlo Erba), in order to weigh the exact amounts of cations. The final concentration of each cation (typically in the 0.5 – 1M range) was finally determined by a colorimetric titration method already detailed in our previous works [20].

The precipitation of hydroxide precursors was based on the protocol already reported for the preparation of $UO_2.nH_2O$ by Martinez *et al.* [21]. In the case of $Ce_{0.8}Ln_{0.2}O_{1.9}$ samples (Ln = Nd, Sm, Gd), the precipitation of the hydroxide precursors was performed by mixing trivalent cerium and chosen lanthanide cation in nitric acid, in the desired stoichiometric ratio x = Ln/(Ce + Ln). The mixture of cations was then poured into a large excess (400%) of 2M NH_4OH solution at room temperature, leading to the instantaneous formation of a yellowish precipitate. This latter was further maintained under magnetic stirring for one hour. Afterwards, the powders were centrifuged at 4500 rpm, then washed twice with deionized water then once with ethanol in order to get rid of any traces of NH_4OH.

Finally, a mechanic treatment was applied to the samples with the aim to avoid aggregation of the powders that can further decrease their sintering capability. Samples were then mixed with 50 mL of ethanol, well-known solvent used in de-agglomeration processes [22], and poured into a flask. The suspension was then stirred mechanically at 40°C under

vacuum until the solvent was fully evaporated. A similar protocol was followed for the $Th_{1-x}Y_xO_{2-x/2}$ samples series, starting with a mixture of Th^{4+} and Y^{3+} in nitric acid media.

The precise chemical composition of the powdered samples was further evaluated by two different methods (Table 1). For the $Th_{1-x}Y_xO_{2-x/2}$ series, a small amount of powder was first dissolved in aqua regia, then diluted in 1% HNO_3 before ICP-AES (Spectro Arcos EOP) measurements (protocols for solution sampling and further analysis have been already described in our previous publication [23]). The emission bands chosen were 401.913, 283.730 and 274.716 nm for thorium, and 371.030 and 324.2278 nm for yttrium concentration determination. For the $Ce_{0.8}Ln_{0.2}O_{1.9}$ series, the compositions were determined from Energy Dispersive Spectrometry (EDS) analyses coupled with the SEM device, using a Bruker AXS X-Flash 5010 detector. Each powdered sample was embedded in an epoxy resin, polished to the 1 µm grid and carbon coated prior analyses. EDS results were then obtained from around 10 different analyses. At least 400000 counts spectra were collected by the EDS detector using routinely an optimal working distance of 11.4 mm and an acceleration voltage of 15 kV.

Whatever the sample under consideration, weight percentages of cations and associated molar ratios were then determined and found in very good agreement with the values expected. One can then assume that the precipitation of both tetravalent and trivalent cations was quantitative using the hydroxide route for the two systems investigated.

Table 1. Weight percentages of the cations and associated molar ratios in the as-synthesized $Th_{1-x}Y_xO_{2-x/2}$ (ICP-AES measurement) and $Ce_{1-x}Ln_xO_{2-x/2}$ (X-EDS) sample series.

ICP-AES	**$Th_{1-x}Y_xO_{2-x/2}$**	**$x_{calc.}$**	**Th (wt.%)**	**Y (wt.%)**	**$x_{exp.}$**
		0.08	84.6 ± 0.9	2.9 ± 0.2	0.08 ± 0.01
		0.15	82.1 ± 2.2	5.9 ± 0.6	0.14 ± 0.02
X-EDS	**$Ce_{0.8}Ln_{0.2}O_{1.9}$**	**Ln**	**Ce (wt.%)**	**Ln (wt.%)**	**$x_{exp.}$**
		Nd	62.2 ± 0.3	20.1 ± 0.3	0.23 ± 0.01
		Sm	65.9 ± 0.5	19.0 ± 1.5	0.21 ± 0.02
		Gd	63.4 ± 1.8	19.1 ± 2.5	0.21 ± 0.03

Characterization.

Powder X-Ray Diffraction (PXRD) diagrams were recorded with a Bruker D8 apparatus at Cu $K\alpha_{1,2}$ radiation (λ = 1.54184 Å). Patterns were collected in the $5° \leq 2\theta \leq 120°$ domain, with a step size of $\Delta(2\theta) = 0.03°$ and a total counting time of about 2.5 hours.

Rietveld refinement were further performed with the Cox-Hastings pseudo-Voigt profile function [24] of the Fullprof_suite program [25].

Scanning Electron Microscope (SEM) observations of powders were performed directly on raw samples using a FEI Quanta 200 apparatus. High vacuum conditions and low accelerating voltage (2 – 3.1 kV) were selected to obtain high resolution images. In parallel, TEM observations and EDS analyses were performed with a JEM-2200FS microscope coupled with a JEOL SDD 30 mm^2 HyperNine (138 eV) spectrometer. Sample preparation consisted in the deposition of a drop of powder suspension in ethanol on a carbon copper grid.

Finally, specific surface area of the samples was measured by the BET method using a Micromeritics Tristar 3020. Samples were first outgassed at 90°C under vacuum for 4 hours before measurement.

Thermal analyses and sintering.

Thermogravimetric analyses and dilatometric measurements were conducted on Setaram Setsys Evolution apparatus. For TGA, about 20 mg were placed into an alumina crucible, then weight loss was recorded between room temperature and 1000°C (heating rate : 10°C.min^{-1}) under air. For dilatometry, heat treatment was maintained up to 1600°C then a dwell time of 30 minutes was applied. In each case, samples were cooled down to room temperature at 30°C.min^{-1}.

Finally, the densification state of the pellets was estimated through geometrical measurements. The average of at least ten values of pellets thickness and diameter, obtained thanks to a precision calliper, was considered to calculate the relative density, which is correlated to the global porosity of the samples.

3. Results and discussion

Characterization of the powdered samples.

Powder samples prepared from the co-precipitation through the hydroxide route of thorium and yttrium, on the one hand, and of cerium and trivalent lanthanides, on the other hand, were first characterized by PXRD analyses (Figure 1). For both samples series, the patterns exhibited all the PXRD lines of the fluorite-type structure (cubic, Fm-3m space group) which is characteristic of ThO_2 [26] and CeO_2 [12] compounds. The synthesis process then did not end up with the formation of Th- or Ce-based hydroxides but with the precipitation of hydrated oxides. In the case of thorium, and more generally for all tetravalent actinides, similar results were already reported in the literature [27], and described as the initial formation of hydroxide colloids [28], followed by an aging step leading to hydrated oxide compounds as follows, eventually through the formation of $AnO(OH)_2.nH_2O$ as an intermediate [29] :

$$An^{4+} + 4\ OH^- \leftrightarrow An(OH)_4 \leftrightarrow AnO_2\ .\ xH_2O + (2\text{-}x)\ H_2O \qquad (1.)$$

When dealing with Ce-based samples, several authors also mentioned the formation of hydrated cerium oxides, for example from the thermal hydrolysis of Ce^{4+} in aqueous solution. Quite similarly to tetravalent actinides, intermediate complexes with the form $[Ce(OH)_x(H_2O)_y]^{(4-x)+}$ are formed and further give rise to $CeO_2.nH_2O$ [30]. However, it is important to note that this process is much more favourable for Ce^{4+} ions compared to Ce^{3+} (due to the more important tendency of the former one to hydrolyse considering its higher charge and smaller radius size). On this basis, it is more likely that, in our system, the reaction first proceeded through the oxidization of Ce^{3+} into Ce^{4+}, then through the hydrolysis of this latter. Such oxidization was already reported to occur for trivalent cerium in aqueous solution, in presence of various complexing and/or shaping agents such ammonia, urea or hexamethylenetetramine [31].

For all the prepared samples, the PXRD lines exhibited a large width, associated to a poor crystallization state and/or to a particle size in the nanometer range. Indeed, Rietveld refinement of the PXRD patterns generally led to an average crystallite size (i.e. coherent length domains), of about 1-2 nm. Also, it is important to note that no additional PXRD lines

were detected in the patterns, such as those of Ln_2O_3 sesquioxides [32], indicating that the trivalent elements considered in this work (i.e. Y^{3+} or Ln^{3+}) were co-precipitated along with Th^{4+} and Ce^{4+} then did not segregate during the aging of the hydroxide colloids.

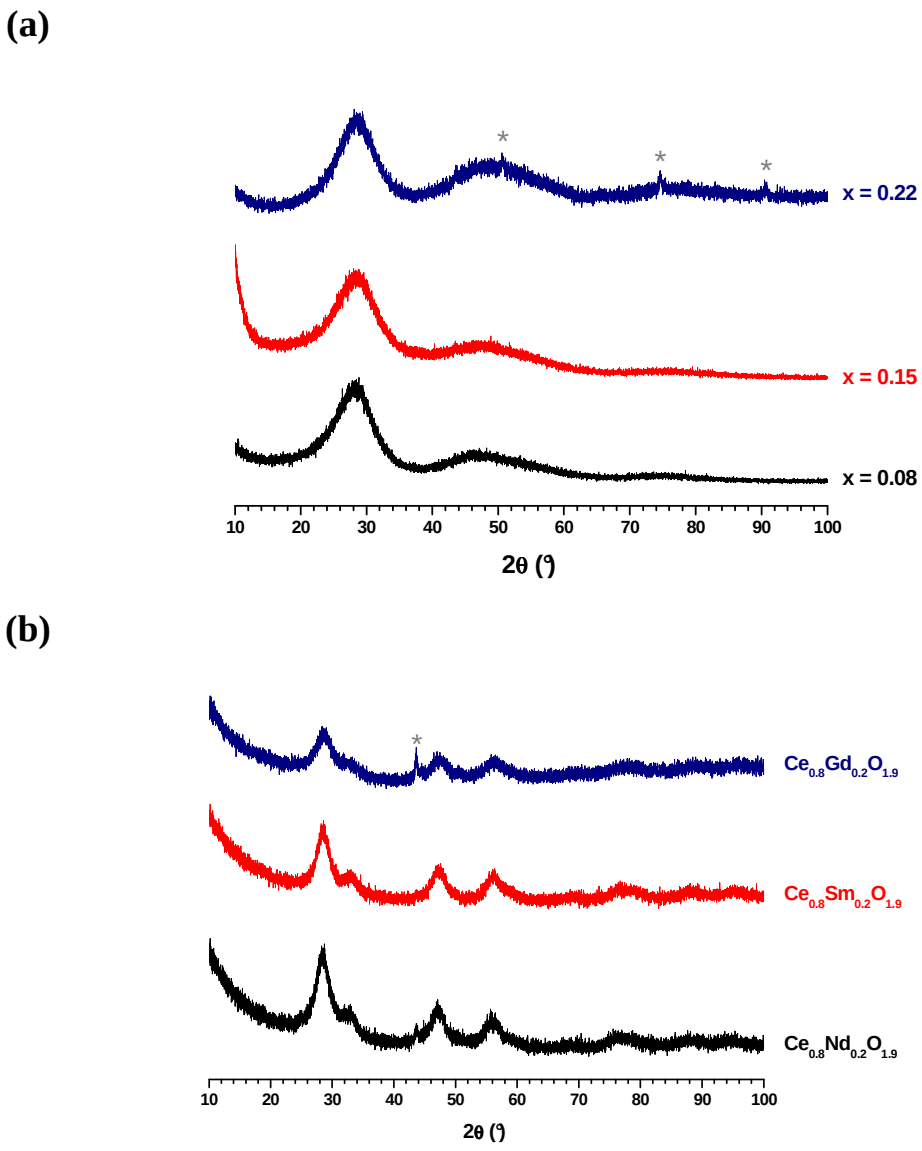

Figure 1. PXRD patterns of the as-synthesized samples in the $Th_{1-x}Y_xO_{2-x/2}$ (a) and $Ce_{0.8}Ln_{0.2}O_{1.9}$ (b) series (* symbols mark the PXRD lines of the sample holder).

The morphology of the (Ce,Ln^{III}) and (Th,Y) hydrated oxides was then explored by both scanning (SEM) and transmission (TEM) electron microscopies. For the two sample series considered, SEM micrographs (Figure 2) exhibit a similar habit, with the powders being composed of very small particles. Due to the resolution limit of the SEM apparatus in the observations conditions, it was not possible to precisely estimate their size, which obviously

remained lower than 10 nm. Moreover, despite the drying step performed under vacuum, one can still observe the formation of large aggregates of about 10-20 µm. Nevertheless, they could arise from the deposition of the powders on carbon sticks prior to observation and/or from the high vacuum conditions used during image recording.

In spite of this partial aggregation, the very high reactivity of the samples was confirmed by specific area values which all ranged between 130 and 180 $m^2.g^{-1}$ for the $Ce_{0.8}Ln_{0.2}O_{1.9}\cdot nH_2O$ compounds, while they could reach up to 230 $m^2.g^{-1}$ for the Th-based samples. However, it appeared difficult to establish a clear trend between the chemical composition of the samples and their specific surface area. Most probably, the surface is essentially dependent on the drying process performed under vacuum, and can vary sensibly from one batch to another. Nevertheless, all the studied samples presented a surface significantly higher than 100 $m^2.g^{-1}$, which can be used to improve the sintering properties of these compounds and control their final microstructure, typically to obtain dense and fine-grain microstructures [33].

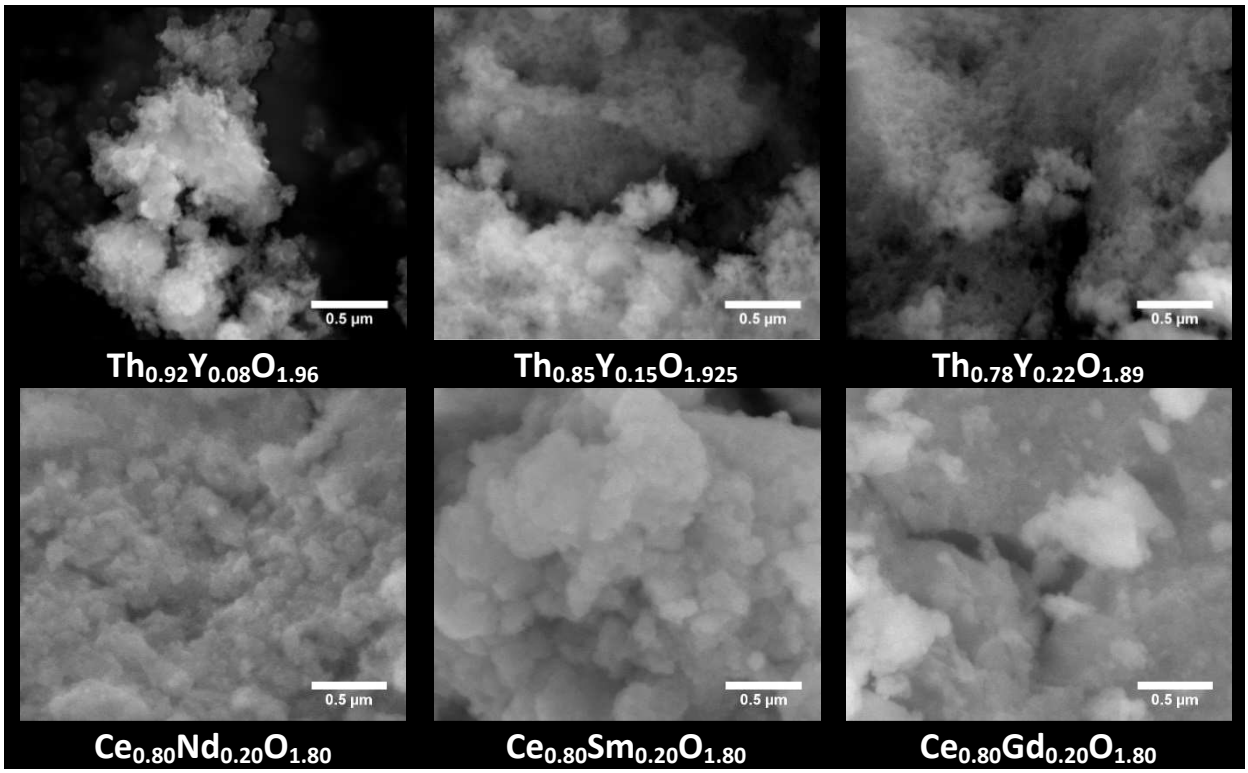

Figure 2. SEM micrographs of as-synthesized powders in the $Th_{1-x}Y_xO_{2-x/2}$ and $Ce_{1-x}Ln_xO_{2-x/2}$ series.

Finally, additional TEM micrographs were recorded in order to precisely estimate the size of the elementary particles constituting the samples and their chemical composition

(Figure 3). All the images collected accounted for nanosized powders in the two series of samples prepared. Indeed, the crystallites generally reached 2 to 5 nm and further aggregate to form agglomerates of about 10-20 nm. This result can be considered to be in good agreement with those obtained through PXRD Rietveld refinement, owing to the uncertainties of both techniques.

Qualitative EDS analyses were also performed on the crystallites, and confirmed the simultaneous presence of tetravalent (i.e. Th^{4+} or Ce^{4+}) and trivalent (Y^{3+} or Gd^{3+}) elements. This result confirmed that the protocol developed for the preparation of the powders led to the co-precipitation of the cations as hydrated based oxides solid solutions without any segregation of the trivalent cations. One can then expect the formation of very homogenous compounds after sintering, which in some cases cannot be obtained by other wet chemistry routes. As a matter of example, the preparation of $Th_{1-x}Y_xO_{2-x/2}$ oxides was frequently reported through an initial step of oxalic precipitation [34]. However, for $x > 0.15$, polyphase oxalate systems can be obtained and further led to heterogeneities in the cation distribution after conversion at high temperature [35]. The use of the so-called hydroxide route could then be considered as an easy and direct path towards highly reactive and homogeneous oxide based powders with the general formula $M^{IV}_{1-x}M^{III}_xO_{2-x/2}$.

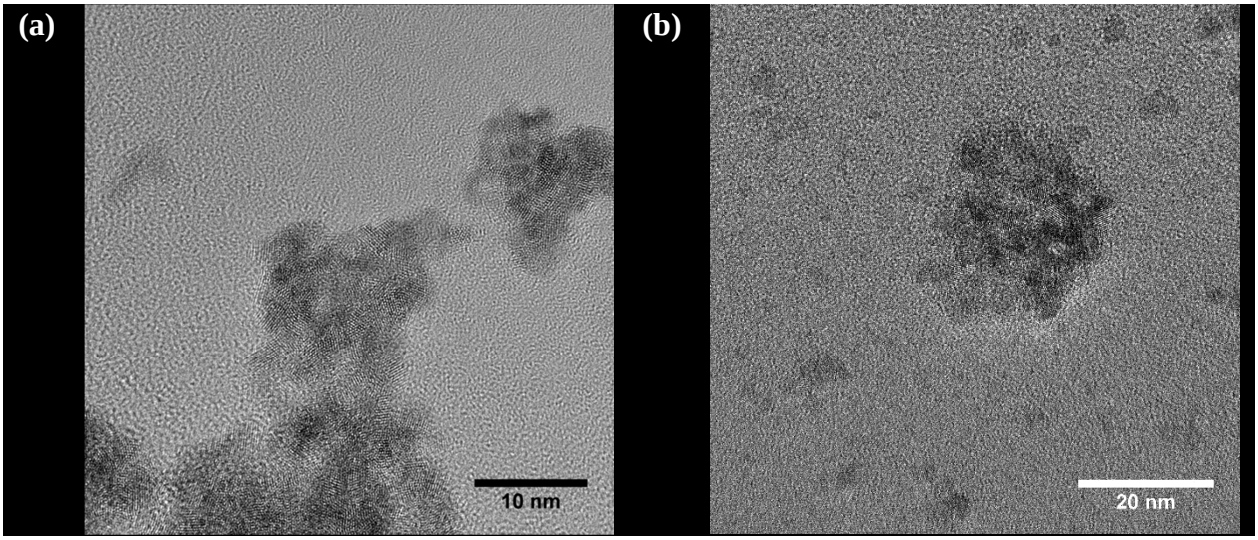

Figure 3. TEM micrographs of $Th_{0.92}Y_{0.08}O_{1.96}\cdot nH_2O$ (a) and $Ce_{0.8}Gd_{0.2}O_{1.9}\cdot nH_2O$ (b) samples.

Thermal behaviour.

The second part of this work was devoted to the conversion of hydrated precursors into anhydrous $Th_{1-x}Y_xO_{2-x/2}$ and $Ce_{0.8}Ln_{0.2}O_{1.9}$ oxides through heat treatment at high temperature. In this aim, all the prepared samples were first analyzed by TGA in order to estimate their initial hydration state and to assess the dehydration process. Whatever the type of sample studied and its chemical composition, the general aspect of the thermograms remained very similar (Figure 4). Indeed, the weight loss systematically appeared to be very progressive up to 500-600°C, where the anhydrous oxide form is obtained, even if a more rapid dehydration was observed at the onset of the heat treatment, i.e. from room temperature to 200°C. Such behavior is consistent with previous studies performed on $MO_2.nH_2O$ compounds with M = U, Th or Ce, which also exhibited progressive dehydration rather than sharp transition from the hydrated oxide precursor to the final anhydrous form [36].

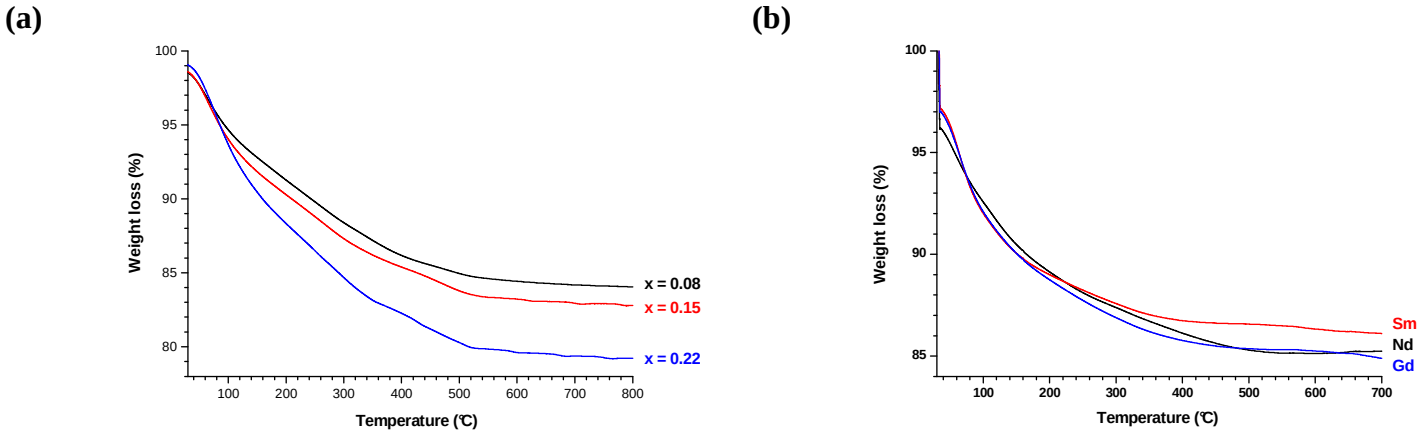

Figure 4. TG analyses recorded for $Th_{1-x}Y_xO_{2-x/2}\cdot nH_2O$ (a) and $Ce_{0.8}Ln_{0.2}O_{1.9}\cdot nH_2O$ (b) samples.

The total weight loss recorded for the various samples studied also appeared to be in the same range of magnitude, *i.e.* between 13 and 20%. For the $Ce_{0.8}Ln_{0.2}O_{1.9}\cdot nH_2O$ series, it corresponds to a value of n = 3 – 3.5, which do not seem to be strongly dependent on the trivalent dopant. Conversely, the hydration state of the $Th_{1-x}Y_xO_{2-x/2}\cdot nH_2O$ oxides was found to slightly vary with the amount of yttrium incorporated; the n value increasing from 3.5 for x = 0.08 to 4.4 for x = 0.22. Nevertheless, it is to note that the total amount of water measured in the hydrated oxides exceeds from far what could be expected from the aging of an initial hydroxide compound. Indeed, as described in equation (1), the maximum value of n should be 2, while the various works reported on tetravalent actinide oxides frequently reported samples with the general formula $An^{IV}O_2.H_2O$ or $An^{IV}O_2.2H_2O$ [37]. On this basis, two types of water

molecules could be present in our samples. On the one hand, adsorbed water is expected to be present due to the very high specific surface area of the samples, and is probably eliminated in the first part of the heat treatment, i.e. below 200°C. On the other hand, constitutional water, which comes from the aging process of the initial hydroxide, is probably eliminated at higher temperature, typically between 200 and 600°C. However, as the weight loss was found to be very progressive, it was not possible to discriminate and to quantify these two kinds of water content in this work.

The variation of the crystal structure was further monitored versus temperature. In this aim, a heat treatment of 6 hours was performed at various temperatures on the $Th_{0.92}Y_{0.08}O_{1.96}$ sample (Figure 5). As already described in the first section, the PXRD pattern recorded at room temperature only presented broad peaks, still characteristic of the ThO_2 based solid solutions. After heating at 500°C, i.e. after the complete dehydration of the sample, the same PXRD peaks were observed, although the departure of constitutional water is likely to provoke a slight shift in their position. Also, a significant decrease of their FWHM, indicating an increase of the average crystallite size (coherent domain length) was observed. Indeed, growth phenomena can proceed even at low temperature, for example from the mechanical rearrangement of adjacent crystallites, frequently referred to as 'oriented attachment' (OA) [38]. Oriented attachment is further probably still responsible for the narrowing of PXRD lines observed up to 1000°C.

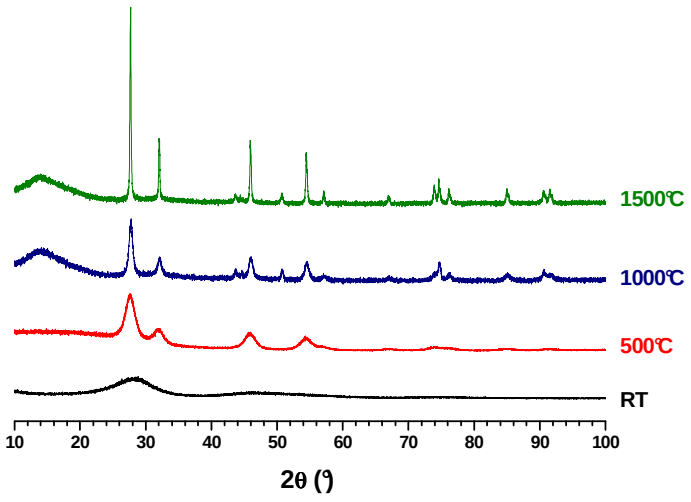

Figure 5. Variation of the PXRD pattern of $Th_{0.92}Y_{0.08}O_{1.96}\cdot nH_2O$ versus the heating temperature.

For higher temperatures, the decrease of the FWHM was even more pronounced and was once again correlated to an increase of the average crystallite size due to solid state diffusion processes. Indeed, OA and diffusion mechanisms were recently reported to occur successively during the sintering of CeO_2 and ThO_2 microspheres [39] and probably act similarly during the heat treatment of $Th_{1-x}Y_xO_{2-x/2}$ and $Ce_{0.8}Ln_{0.2}O_{1.9}$ solid solutions [40].

The growth of the crystallites within the powder samples during heat treatment was also correlated to the variation of the specific surface area, evaluated by the BET method after firing at various temperatures (Figure 6). One can note that specific surface drastically decreased between room temperature and 500°C, while the PXRD pattern only exhibited moderate narrowing of the FWHM. Hence, the decrease of the specific surface area in this temperature range is surely linked to a strong agglomeration of nanometric particles under dehydration. The growth of the particles, which occurs at higher temperatures due to oriented attachment and diffusion mechanisms, then accounts for a smaller decrease of the specific surface area, typically from about 30 to less than 1 $m^2.g^{-1}$ between 500 and 1500°C.

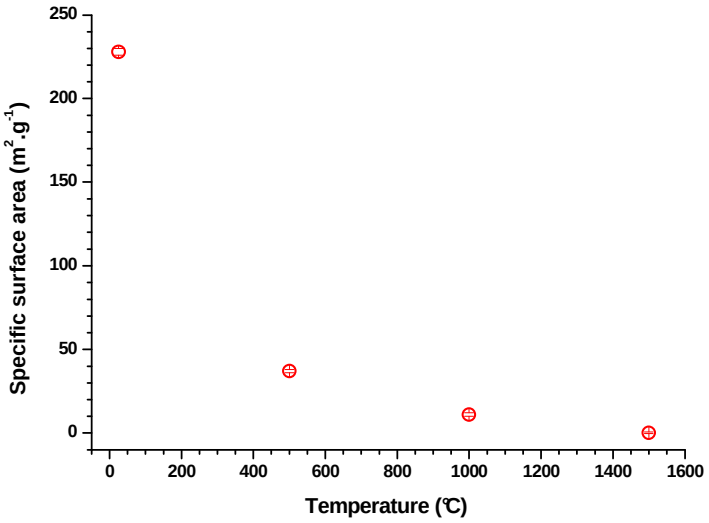

Figure 6. Variation of the specific surface area versus heating temperature obtained for $Th_{0.92}Y_{0.08}O_{1.96}\cdot nH_2O$.

Sintering capability.

The sintering of the samples was finally investigated in a last step, in order to prepare dense ceramic materials with fine grain microstructure. Indeed, densities above 97% are generally required to ensure good electrical properties (i.e. to avoid undesired resistivity due

to closed porosity) while submicrometric grains are frequently correlated to good mechanical properties. Owing to the direct precipitation of the samples as hydrated mixed oxides, on the one hand, and to the loss of reactivity observed upon heating, particularly through the drastic drop of the specific surface area, the sintering of the powders was performed without any preliminary heat treatment. Raw powders were then shaped as cylindrical pellets (Ø = 5-8 mm) by uniaxial pressure (600 MPa), leading to green density of about 40 to 50 % of the theoretical value.

Dilatometric analyses were then performed in order to estimate the sintering temperature of the pellets prepared (Figure 7). Whatever the chemical composition of the sample considered, both within the $Ce^{IV}_{1-x}Ln^{III}_{x}O_{2-x/2}$ or the $Th_{1-x}Y_xO_{2-x/2}$ series, the linear shrinkage systemically exhibited two different steps. The first one, starting from the beginning of the heat treatment to about 500°C, was correlated to the dehydration of the powders. It resulted in a linear shrinkage of around 10-15%, corresponding to a significant volume shrinkage which might lead to the formation of cracks within the pellet. Hence, the heating profile must be thoroughly adapted to ensure the complete dehydration of the oxide samples without compromising the mechanical integrity of the pellet.

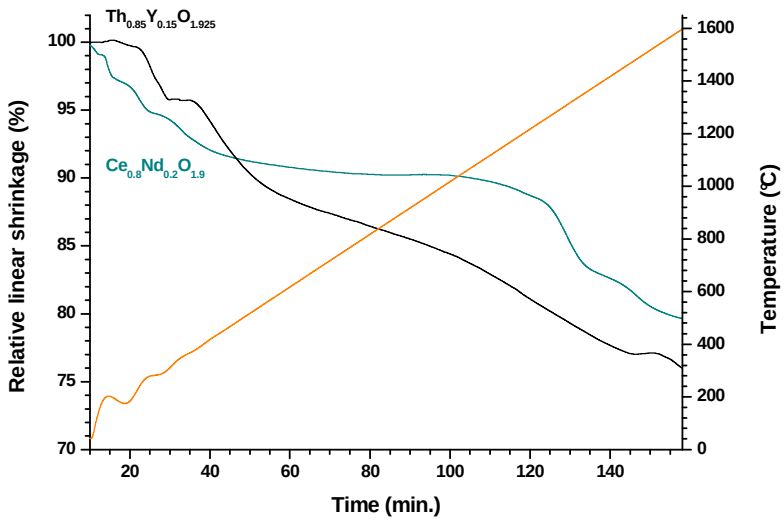

Figure 7. Dilatometric curves obtained for $Ce_{0.8}Nd_{0.2}O_{1.9}$ (green) and $Th_{0.85}Y_{0.15}O_{1.925}$ (black) samples.

The second shrinkage step was found to be very progressive and started slightly above 1000°C. One can then assume that it corresponds both to the densification of the pellet and to grain growth processes which are enhanced due to the nanosized character of the starting

powder. Also, one can note that between 1200 and 1500°C, the densification of Ce-based solid solutions proceeded faster than for thoria-based materials, which can be assigned to the higher sintering temperature generally reported for ThO_2 (i.e. in the 1500-1600°C range [41]) compared to CeO_2 (around 1400°C [42]). However, the densification of both samples was not completed at 1600°C, meaning that higher temperature of heat treatment and/or longer holding time are required to obtain highly dense samples.

On this basis, the sintering conditions leading to the full densification of the pellets, as well as the associated microstructure in term of grain size, were more specifically investigated for the $Th_{1-x}Y_xO_{2-x/2}$ samples series. In this aim, pellets were heated at 1500°C or 1600°C, considering holding times ranging between 1 and 8 hours. Moreover, heating rate of 5°C.min^{-1} as well as a 2 hours dwell at 300°C were considered to prevent the formation of cracks in the pellets. As expected from the dilatometric study, the relative density of the samples was found to increase with the heating time for the two temperatures considered (Figure 8). Nevertheless, heat treatment at 1600°C rapidly led to highly densified samples, i.e. typically with d > 95% TD, even though if the highest yttrium content studied was initially associated to significantly lower density values, probably due to solute drag effects slowing down the motion of grain boundaries [43].

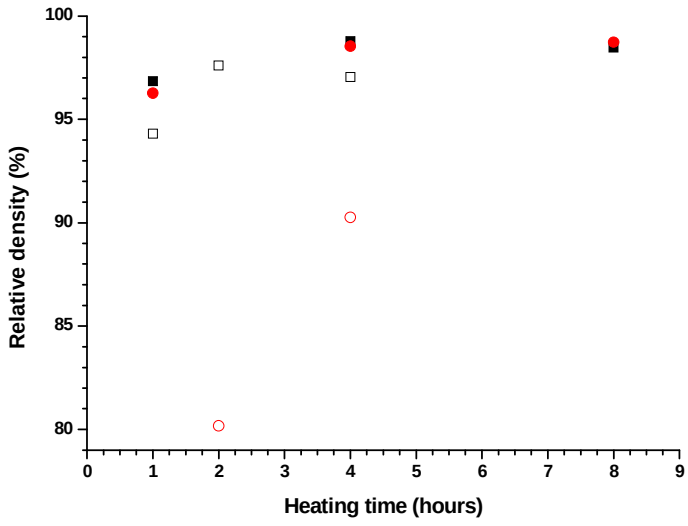

Figure 8. Evolution of the relative density of $Th_{0.85}Y_{0.15}O_{1.925}$ (black) and $Th_{0.78}Y_{0.22}O_{1.89}$ (red) samples during their sintering at 1500°C (open symbols) and 1600°C (full symbols).

This result can be compared with those recently reported for the sintering of $Th_{1-x}Y_xO_{2-x/2}$ powders initially prepared through oxalic co-precipitation and subsequent thermal conversion [43]. In the present study, the initial important reactivity of the hydrated oxide powder did not lead to a significant decrease of the sintering temperature. Nevertheless, the density achieved after only 1 hour of heat treatment at 1600°C already reached more than 95%TD while it was below 90% for the powders prepared from oxalic precipitation. On this basis, the very high specific surface area offered by the hydroxide route led to the strong increase of the densification kinetics during the first hours of heat treatment at high temperature.

The SEM micrographs recorded on polished sections of samples sintered at 1600°C for 4 and 8 hours confirmed the very good densification state of the pellets (Figure 9). Indeed, no significant porosity was observed at the surface of the samples, neither in intra- nor in inter-granular position. Moreover, the grain size was estimated by image analysis of all the sintered samples and was typically found between 100 and 500 nm whatever the chemical composition. It did not seem to significantly evolve when increasing the heating time at 1600°C. Once again, these values appear to be in the same order of magnitude than those reported when working with oxalate precursors [43]. This observation thus confirms that the sintering process is rapidly marked by a strong grain growth step, which probably proceeds concomitantly to the densification. Once the grains big enough (i.e. tens of nanometers), their growth kinetics probably slowed down and became comparable to that observed on similar systems prepared through alternative chemical routes.

Also, it is to note that the initial nanosize character of the grain did not generate an enhanced migration of the trivalent elements to the grain boundaries. Indeed, this typical behavior was frequently reported during heat treatment of $M^{IV}_{1-x}M^{III}_xO_{2-x/2}$ (with M^{IV} = Ce, Th and M^{III} = La-Yb) fluorite-type solid solutions [44], and resulted in solute drag effect that can slow down, if not hinder, the sintering and grain growth processes. In our study, the important occurrence of grain boundaries in the starting powdered compact did not result in such an effect since a full densification of the pellets was stated after heating at 1600°C. On this basis, the initial co-precipitation of tri- and tetravalent lanthanide and actinide cations through the hydroxide route successfully allowed the direct sintering of the as-synthesized powders and ended up with ceramics exhibiting microstructural features of interest for their application as electrolyte materials, i.e. high density associated to submicrometric grain size.

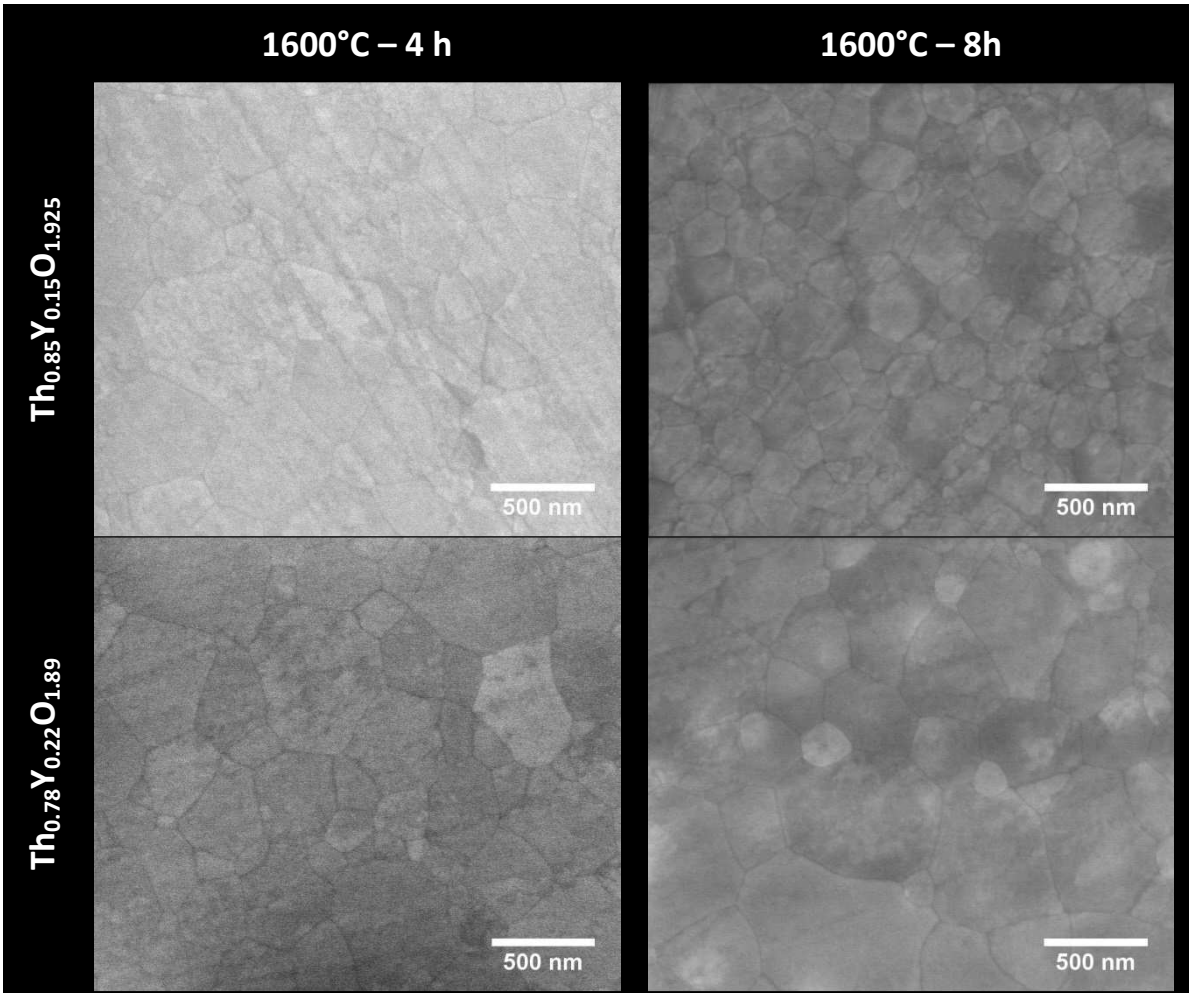

Figure 9. SEM micrographs of $Th_{0.85}Y_{0.15}O_{1.925}$ and $Th_{0.78}Y_{0.22}O_{1.89}$ sintered samples.

4. Conclusion

Highly reactive and nanosized $Th_{1-x}Y_xO_{2-x/2}$ or $Ce_{0.8}Ln_{0.2}O_{1.9}$ mixed oxides were prepared through the initial precipitation of hydroxide precursors which were further dried under vacuum. Whatever the chemical system investigated, i.e. $Th_{1-x}Y_xO_{2-x/2}$ or $Ce_{0.8}Ln_{0.2}O_{1.9}$, the characterization of the powdered samples evidenced a rapid aging process leading to hydrated oxides. Moreover, the precipitation appeared to be quantitative and no segregation of the trivalent cations was pointed out, either by PXRD or by EDS analyses conducted during TEM observations. The thermal behavior of such hydrated oxides was further explored and first showed a two-step dehydration process, with the successive departure of adsorbed water up to 200°C, followed by that of constitutive water coming from the aging of initial hydroxide colloids, both yielding a drastic drop of the powders reactivity (i.e. decrease of the specific surface area).

Sintering of the samples was then undertaken by starting from raw powders in order to preserve their reactivity. Such a process, composed by the direct shaping of the samples followed by their heat treatment at high temperature, then eliminates potential preliminary steps, such as firing or milling, which can led to safety or pollution issues when handling radioactive materials. Dilatometry experiments coupled to SEM observations and density measurements then pointed out the very rapid densification kinetics. Indeed, if the sintering temperature (1600°C) was not significantly modified compared to other wet-chemistry routes, highly densified pellets above 95%TD were obtained after only 1 hour of heat treatment. The initial preparation of nanosized powders also led to a fine grain microstructure, which is frequently linked to improved physico-chemical properties in use of the ceramics. This easy and versatile precipitation process that can be followed by direct densification of the powders, then appears as a promising option for the elaboration of homogenous ceramic electrolytes. The associated electrical properties are then currently under investigation to assess their potential utilization in SOFC units or in oxygen sensors.

Acknowledgements

The authors would like to thank Johann Ravaux and Renaud Podor for their help during SEM examinations of the samples, as well as Xavier Le Goff for his support during TEM observations. Y. Cherkaski and J. Martinez are grateful to CEA for its continuous financial support and for funding their PhD thesis.

References

[1] S. H. Holmes, C. F. Reinhart, *Build Res Inf* **2013**, *41*, 209-222.

[2] I. L. Pioro, *Handbook of Generation IV Nuclear Reactors*, Woodhead Publishing, **2016**.

[3] J. E. Kelly, *Prog Nucl Energ* **2014**, *77*, 240-246.

[4] L. Brissonneau, *J Nucl Mater* **2012**, *423*, 67-78.

[5] E. Schouler, A. Hammou, M. Kleitz, *Mater Res Bull* **1976**, *11*, 1137-1146.

[6] D. J. Hayes, *J Phys E Sci Instrum* **1974**, *7*, 69-75.

[7] I. C. Cosentino, R. Muccillo, *Mater Lett* **2001**, *48*, 253-257.

[8] R. G. Taylor, R. Thompson, *J Nucl Mater* **1983**, *115*, 25-38.

[9] Q. A. Huang, R. Hui, B. W. Wang, H. J. Zhang, *Electrochim Acta* **2007**, *52*, 8144-8164.

[10] A. B. Stambouli, E. Traversa, *Renew Sust Energ Rev* **2002**, *6*, 433-455.

[11] R. Ramamoorthy, P. K. Dutta, S. A. Akbar, *J Mater Sci* **2003**, *38*, 4271-4282.

[12] D. Horlait, L. Claparède, N. Clavier, S. Szenknect, N. Dacheux, J. Ravaux, R. Podor, *Inorg Chem* **2011**, *50*, 7150-7161.

[13] D. Prieur, A. Jankowiak, C. Leorier, N. Herlet, L. Donnet, P. Dehaudt, C. Maillard, J. P. Laval, P. Blanchart, *Powder Technol* **2011**, *208*, 553-557.

[14] H. Inaba, H. Tagawa, *Solid State Ionics* **1996**, *83*, 1-16.

[15] F. Abraham, B. Arab-Chapelet, M. Rivenet, C. Tamain, S. Grandjean, *Coord. Chem. Rev.* **2014**, *266-267*, 28-68.

[16] a) W. Huang, P. Shuk, M. Greenblatt, *Solid State Ionics* **1997**, *100*, 23-27; b) C. Laberty-Robert, J. W. Long, E. M. Lucas, K. A. Pettigrew, R. M. Stroud, M. S. Doescher, D. R. Rolison, *Chem Mater* **2006**, *18*, 50-58.

[17] J. Martinez, F. Audubert, N. Clavier, N. Dacheux, *Vol. FR3016360*, **2015**.

[18] M. Aizenshtein, T. Y. Shvareva, A. Navrotsky, *J Am Ceram Soc* **2010**, *93*, 4142-4147.

[19] a) V. P. Kumar, Y. S. Reddy, P. Kistaiah, G. Prasad, C. V. Reddy, *Mater Chem Phys* **2008**, *112*, 711-718; b) M. Dudek, *J Eur Ceram Soc* **2008**, *28*, 965-971.

[20] N. Clavier, N. Dacheux, P. Martinez, V. Brandel, R. Podor, P. Le Coustumer, *J Nucl Mater* **2004**, *335*, 397-409.

[21] J. Martinez, N. Clavier, A. Mesbah, F. Audubert, X. F. Le Goff, N. Vigier, N. Dacheux, *J Nucl Mater* **2015**, *462*, 173-181.

[22] K. Ananthasivan, S. Anthonysamy, A. Singh, P. R. Vasudeva Rao, *J Nucl Mater* **2002**, *306*, 1-9.

[23] D. T. Costin, A. Mesbah, N. Clavier, S. Szenknect, N. Dacheux, C. Poinssot, J. Ravaux, H. P. Brau, *Prog Nucl Energ* **2012**, *57*, 155-160.

[24] P. Thompson, D. E. Cox, J. B. Hastings, *J Appl Crystallogr* **1987**, *20*, 79-83.

[25] C. Frontera, J. Rodriguez-Carvajal, *Phys B-Cond Matter* **2003**, *335*, 219-222.

[26] S. Hubert, J. Purans, G. Heisbourg, P. Moisy, N. Dacheux, *Inorg Chem* **2006**, *45*, 3887-3894.

[27] V. Neck, J. I. Kim, *Radiochim Acta* **2001**, *89*, 1-16.

[28] G. R. Choppin, *J Radioanal Nucl Ch* **2007**, *273*, 695-703.

[29] a) J. L. Liu, M. B. Luo, Z. Z. Yuan, A. D. Ping, *J Radioanal Nucl Ch* **2013**, *298*, 1427-1434; b) J. M. Haschke, *J Nucl Mater* **2005**, *344*, 8-12.

[30] M. Hirano, M. Inagaki, *J Mater Chem* **2000**, *10*, 473-477.

[31] P. L. Chen, I. W. Chen, *J Am Ceram Soc* **1993**, *76*, 1577-1583.

[32] M. Zinkevich, *Prog Mater Sci* **2007**, *52*, 597-647.

[33] G. M. Christie, F. P. F. van Berkel, *Solid State Ionics* **1996**, *83*, 17-27.

[34] a) T. Reetz, I. Haase, H. Ullmann, H. J. Lang, V. Saly, M. Hartmanova, *Solid State Ionics* **1989**, *36*, 193-195; b) V. Jayaraman, D. Krishnamurthy, R. Ganesan, A. Thiruvengadasami, R. Sudha, M. V. R. Prasad, T. Gnanasekaran, *Ionics* **2007**, *13*, 299-303.

[35] M. Gabard, Y. Cherkaski, N. Clavier, L. Brissonneau, M. C. Steil, J. Fouletier, A. Mesbah, N. Dacheux, *J Alloy Compd* **2016**, *689*, 374-382.

[36] O. Yildiz, *J Nucl Mater* **2007**, *366*, 266-271.

[37] a) G. I. Nkou Bouala, N. Clavier, R. Podor, J. Cambedouzou, A. Mesbah, H. P. Brau, J. Léchelle, N. Dacheux, *Crystengcomm* **2014**, *16*, 6944-6954; b) R. J. Finch, R. C. Ewing, *J Nucl Mater* **1992**, *190*, 133-156; c) A. E. V. Gorden, M. L. McKee, *J Phys Chem A* **2016**, *120*, 8169-8183.

[38] P. Scardi, M. Leoni, M. Mueller, R. Di Maggio, *Mat Sci Eng a-Struct* **2010**, *528*, 77-82.

[39] a) G. I. Nkou Bouala, N. Clavier, J. Léchelle, J. Monnier, C. Ricolleau, N. Dacheux, R. Podor, *J Eur Ceram Soc* **2016**; b) G. I. Nkou Bouala, N. Clavier, S. Martin, J. Lechelle, J. Favrichon, H. P. Brau, N. Dacheux, R. Podor, *J Phys Chem C* **2016**, *120*, 386-395.

[40] L. Claparede, N. Clavier, N. Dacheux, P. Moisy, R. Podor, J. Ravaux, *Inorg Chem* **2011**, *50*, 9059-9072.

[41] T. R. G. Kutty, K. B. Khan, P. V. Hegde, J. Banerjee, A. K. Sengupta, S. Majumdar, H. S. Kamath, *J Nucl Mater* **2004**, *327*, 211-219.

[42] J. F. Baumard, C. Gault, A. Argoitia, *J Less-Common Met* **1987**, *127*, 125-130.

[43] Y. Cherkaski, N. Clavier, L. Brissonneau, R. Podor, N. Dacheux, *J Eur Ceram Soc* **2017**, *37*, 3381-3391.

[44] a) V. Belliere, G. Joorst, O. Stephan, F. M. F. de Groot, B. M. Weckhuysen, *J Phys Chem B* **2006**, *110*, 9984-9990; b) D. Horlait, N. Clavier, S. Szenknect, N. Dacheux, V. Dubois, *Inorg Chem* **2012**, *51*, 3868-3878; c) D. Horlait, N. Clavier, N. Dacheux, R. Cavalier, R. Podor, *Mater Res Bull* **2012**, *47*, 4017-4025.